Study on the influence mechanism of fin structure on the filling performance of cold adsorption hydrogen storage tank

Jiahao Wang[a,b], Daniele Melideo[a *], Lorenzo Ferrari [a], Paolo Taddei Pardelli [c], Xiaomin Liu [b], Umberto Desideri [a*]

[a] Department of Energy, Systems, Territory and Constructions Engineering, University of Pisa, Largo Lucio Lazzarino, Pisa, 56122, Italy

[b] School of Energy and Power Engineering, Xi'an Jiaotong University, Xi'an 710049, China

[c] Spike Renewables Srl, Viale Manfredo Fanti, 217, 50137, Firenze, Italy

Abstract: Activated carbon cold adsorbed H_2 storage (CAH2) is a promising physical hydrogen storage method. However, conventional storage tanks face problems of local high heat accumulation during the cold adsorption process, leading to low hydrogen storage efficiency and capacity. This study is the first attempt to add high thermal conductivity fins to a conventional CAH2 tank to enhance heat and mass transfer, thereby promoting the hydrogen adsorption process. An accurate mathematical model and finite element method are established to calculate the CAH2 process. The influence mechanism of different fin arrangements, fin length, fin number (spacing), and fin width on the temperature field, adsorption concentration field and storage performance are explored. The results show that adding fins can effectively promote heat transfer and suppress local high temperature and low adsorption concentration areas. When the adsorption mass reaches 0.05kg, the storage efficiency of the three tank schemes with added fins improves by approximately 40% compared with the original tank. Although extending the fin length will enhance heat conduction, it will also suppress the heat convective transfer effect. The optimal fin length is found to be 30mm. Increasing the number of fins (reducing spacing) can significantly decrease the areas of local high temperature and low adsorption concentration, but this beneficial effect diminished when the number of fins exceeded 14. Increasing the fin width has a weaker beneficial effect on the temperature field and adsorption concentration field, and also cause a significant reduction in the tank volume, thereby reducing the total hydrogen storage capacity. The findings of this study can provide important guidance for the application of high thermal conductivity fins in CAH2 tanks.

Keywords: Hydrogen storage; Cold adsorption; Simulation; Fins; Thermal management

1. Introduction

Hydrogen is a highly promising clean and renewable energy source, playing a crucial role in reducing greenhouse gas emissions [1]. However, the efficacious and secure technology for hydrogen storage constitutes a pivotal challenge in the advancement of hydrogen energy systems [2,3]. Currently, the mainstream hydrogen storage methods include three main types: compressing hydrogen at high pressures (350~700 bar); liquefying hydrogen by cryogenic cooling (below -253°C); and solid-state hydrogen storage using chemical compounds (metal hydrides or hydrocarbons) [4, 5]. Compressing hydrogen storage is relatively simple and easy to operate, but the high-pressure operating conditions place higher demands on the required storage tanks, supporting equipment, and storage and transportation safety [6]. Cryogenic liquefaction can achieve more compact hydrogen storage, but the specific equipment and insulation materials required for low temperatures increase storage costs [7]. While hydride storage offers higher safety and hydrogen density, its application is limited by the slow hydrogen absorption and desorption rates, high thermal management requirements, and the low stability of metal hydrides after multiple charging and discharging cycles [8].

To address the challenges of existing hydrogen storage technologies, advanced cold adsorbed H_2 storage (CAH2) at relatively low pressure levels has been proposed. CAH2 is a physical adsorption storage method where hydrogen is adsorbed and stored within the micropores of porous media with large surface areas and extensive gas-solid

interfaces, based on the van der Waals force mechanism [9]. These porous media materials include activated carbon, zeolites, activated carbon fiber (ACF), and metal-organic structures (MOFs), etc. Compared to compressing hydrogen storage, CAH2 allows hydrogen to be stored at relatively low pressures (100 bar or below). It also requires higher temperatures (77K or above) than liquefying hydrogen storage and offers quicker absorption and lower temperature requirements compared to chemical hydrogen storage [10,11]. Related studies also point out that CAH2 shows great application prospects, due to its high-density hydrogen storage and low storage and transportation energy consumption and cost characteristics [12,13]. Therefore, CAH2 technology is considered as one of the most promising storage methods for meeting the goals of the US Department of Energy hydrogen plan for fuel cell powered vehicles [14,15].

The pore characteristics of porous media are crucial factors affecting the adsorption performance of hydrogen. and existing research has explored the adsorption capability of various porous materials [16]. Zhang et al. [17] indicated that the diameter of carbon pores significantly impacts the hydrogen storage capacity of activated carbon, with smaller diameter multi-walled carbon nanotubes showing stronger adsorption capability. Jordá-Beneyto et al. [18] tested a series of porous carbon materials with different pore characteristics, such as chemical activated carbons, carbon nanotubes, carbon fibers, and carbon nanofibers, and found that the hydrogen storage capacity of activated carbon depends on the combination of the micropore volume and the micropore size distribution. Attia et al. [19] developed cross-linked polymer and its porous composites with activated carbon, effectively achieving the excessive absorption of hydrogen. Wang et al. [20] conducted comparative tests on the adsorption performance of various porous medias (COF-105, COF-108, MOF-5, and MOF-177) at room temperature, concluding that MOF-177 had the best adsorption performance. Furukawa et al. [21] used MOF-177 as an adsorption material, achieving an absolute adsorption capacity of up to 11 wt% at 70 bar.

In addition to the material characteristics of porous media, the heat and mass transfer processes within the storage tank also play a crucial role in the hydrogen storage efficiency and capacity in the adsorption process. Hermosilla-Lara et al. [22] found that mechanical energy dissipation accounted for 88% of the total heat generated in the study of thermal effects of activated carbon hydrogen storage tanks, and pointed out that effective heat dissipation measures is necessary to enhance adsorption amount. Momen et al. [23] discovered that the adsorption heat and compression work accompanying the storage process significantly increased the overall temperature of the tank and worsened temperature uniformity, which would severely reduce hydrogen adsorption capacity and efficiency. Additionally, researchers also studied the effects of factors such as initial temperature [24], charge flow rate [25], thermal conductivity [26], and heating power [27] on the hydrogen adsorption process.

Effective thermal management schemes can enhance the efficiency of cold adsorption processes and increase hydrogen storage capacity. Schlemminger et al. [28] used the metal foam bed as heat dissipation enhancement structures in hydrogen storage tanks, significantly accelerating the heat and mass transfer in the adsorption process. Ubaid et al. [29] proposed a flowthrough cooling strategy to reduce the adsorption heat accumulation, showing that this method could effectively expel hot hydrogen in time to keep the hydrogen storage tank at a low temperature. Liu et al. [30] mixed MOF-5 with 10 wt% carbon nanoparticles, increasing the thermal conductivity of MOF-5 by 5 times ($0.56\ W \cdot m^{-1} \cdot K^{-1}$), but a higher thermal conductivity (approximately $3\ W \cdot m^{-1} \cdot K^{-1}$) is needed for sufficient heat dissipation in the storage tank. Tong et al. [31] discussed the effects of charging flow rate, precooling, and flowthrough cooling on the adsorption process, highlighting that combining flowthrough cooling with precooling is an effective method to transfer adsorption heat and improve storage capacity. Ouellet et al. [32] used a genetic algorithm to find the fastest filling method based on the given heat transfer coefficient, target hydrogen storage mass, and adsorbent material characteristics under the constraint of limiting internal temperature and pressure. The above-mentioned thermal management methods all produce certain beneficial effects. However, adding metal foams or high

thermal conductivity nanoparticles has the problems of poor dispersion, low stability after multiple charging and discharging cycles, and high maintenance costs. Additionally, these charging schemes (variable flow rate, precooling, flowthrough cooling) increase the operation complexity of the hydrogen storage and put forward higher requirements for external auxiliary equipment. In contrast, enhancing heat and mass transfer from the perspective of storage tank structural design is a relatively ideal solution and can effectively avoid the aforementioned issues. Currently, there is little research on the application and study of heat dissipation enhancing structures in CAH2 tank, such as adding high thermal conductivity fins and cryogenic cooling tubes. Related research only appeared in the field of solid-state hydrogen storage by chemical compounds [33,34]. Therefore, exploring the benefits of adding high thermal conductivity fins to the hydrogen adsorption process and revealing the influence mechanism on heat and mass transfer process is of great significance for further improving the hydrogen storage performance.

In this context, under the EU-funded Project MAST3RBoost, the Department of Energy, Systems, Territory, and Construction at the University of Pisa, in collaboration with Spike Renewables Srl, is currently engaged in the investigation of CAH2 at low compression levels (100 bar or below). Given the limited thermal management efficiency and hydrogen storage performance of existing CAH2 tank technologies, this study aims to improve the thermal management limitations and enhance hydrogen storage efficiency and capacity. In this study, an accurate computational fluid dynamics model of CAH2 tank is established and verified based on experimental data. Based on the hydrogen filling process of an actual hydrogen refueling station, high thermal conductivity fins are introduced into storage tanks for the first time to explore their effects on high heat accumulation and low adsorption concentration during the adsorption process. The beneficial effect and physical influence mechanism of different fin structure schemes (arrangement, number, width, length) on the adsorption process are analyzed. This study can provide an significant guidance for the application of heat dissipation enhancing structures in the thermal management of CAH2 tanks.

2. CFD model for CAH2

The porous media selected for this study is activated carbon (AC) [35]. When gaseous hydrogen flows in the porous media, it is adsorbed on the pore surface of the AC and transformed into the adsorbed phase, accompanied by the generation of heat. The heat and mass transfer during the hydrogen adsorption by the AC adhere to the mass, momentum, and energy conservation equations.

2.1 Mass conservation

During the adsorption process, the partial differential form of the mass conservation equation in AC tank is expressed as:

$$\frac{\partial\left(\varepsilon_b \rho_g\right)}{\partial t} + \nabla \cdot \left(\rho_g \vec{v}\right) = S_m \tag{1}$$

Where, ρ_g represents the density of hydrogen, ($kg \cdot m^{-3}$); S_m denotes the mass source term, ($kg \cdot m^{-3} \cdot s^{-1}$), which represents the mass of hydrogen converted from the gas state to the adsorbed state per unit volume per second. During the adsorption process, hydrogen converts from the gas state into the adsorbed state, resulting in a decrease in the gas state, thus making S_m negative. The desorption process is opposite. The S_m term for the adsorption process can be expressed as:

$$S_m = -\frac{\partial}{\partial t}\left(\rho_b q_a\right) \tag{2}$$

Where, ρ_b is the AC bed density, and its relationship with the AC porosity ε_b and AC particle density ρ_p is expressed

as: $\rho_b=\rho_p(1-\varepsilon_b)$, (kg AC·m^{-3}); the mass ratio of hydrogen to AC is expressed as: $q_a=M_{H_2}\cdot n_a$, (kg H_2·kg^{-1} AC). Therefore, the mathematical form of the S_m term is:

$$S_m = -\rho_b M_{H_2} \frac{\partial n_a}{\partial t} = -M_{H_2}\left(1-\varepsilon_b\right)\rho_p \frac{\partial n_a}{\partial t} \tag{3}$$

Where, M_{H2} is the molar mass of hydrogen, (kg·mol^{-1}); n_a is the absolute adsorption of hydrogen adsorbed per unit mass of AC, (mol·kg^{-1}).

2.2 Momentum conservation

The momentum conservation of the hydrogen adsorption process in AC tank is described by Darcy's law:

$$\vec{v} = -\frac{\kappa}{\mu}\nabla p \tag{4}$$

Where, $\vec{v}$ denotes the Darcy velocity; the relationship between $\vec{v}$ and the physical velocity $\vec{u}$ of hydrogen in the porous bed is expressed as: $\vec{v} = \varepsilon_b \cdot \vec{u}$; κ represents the permeability; μ denotes the dynamic viscosity.

In the adsorption process, hydrogen is typically regarded as an ideal gas, and its pressure can be calculated using $p=\rho_g RT/ M_{H2}$. For low-velocity flow in porous beds, only viscous resistance needs to be considered. However, for high-velocity flow, both viscous resistance and inertial resistance must be accounted for. Therefore, the Forchheimer equation is used to modify Darcy's law:

$$-\nabla p = \alpha_E \mu \vec{v} + \beta_E \rho_g \|\vec{v}\|\vec{v} \tag{5}$$

Where, α_E denotes the viscous resistance factor, $\alpha_E=150(1-\varepsilon_b)^2/(D_p^2\cdot\varepsilon_b^2)$; β_E denotes the inertial resistance factor, $\beta_E=1.75(1-\varepsilon_b)/(D_p^2\cdot\varepsilon_b^2)$; D_p is the mean particle diameter; $\|\vec{v}\|$ is the module of the Darcy velocity $\vec{v}$. The Forchheimer equation is converted into the form of Darcy's law as follows:

$$\vec{v} = -\frac{\kappa}{\mu}\nabla p \tag{6}$$

$$\kappa' = \frac{2}{\alpha_E + \sqrt{\alpha_E^{\,2} + \left(4\beta_E \rho_g / \mu^2\right)\|\nabla p\|}} \tag{7}$$

2.3 Energy conservation

During the adsorption process by AC, the energy changes are mainly influenced by thermal convection, thermal conduction, compression work, and adsorption heat. The energy conservation equation is expressed as:

$$\left(\rho c_p\right)_{eff}\frac{\partial T}{\partial t} + \rho_g c_{pg}\vec{v}\cdot\nabla T = \nabla\cdot\left(k_{eff}\nabla T\right) + Q + W + \Phi \tag{8}$$

The k_{eff} in the thermal conduction term of Eq.(8) represents the effective thermal conductivity of the AC porous bed:

$$k_{eff} = \varepsilon_b k_g + \left(1-\varepsilon_b\right)k_s \tag{9}$$

Where, kg and ks are the thermal conductivity of hydrogen gas and the porous media, respectively, (W·m^{-1}·K^{-1}).

The effective heat capacity $(\rho c_p)_{eff}$ of the transient term in Eq.(8) considers the heat capacity of the adsorbed hydrogen:

$$\left(\rho c_p\right)_{eff} = \varepsilon_b \rho_g c_{pg} + \left(1-\varepsilon_b\right)\rho_p \left(c_{ps} + q_a c_{pa}\right) = \varepsilon_b \rho_g c_{pg} + \rho_b n_a M_{H_2} c_{pa} + \rho_b c_{ps} \tag{10}$$

The specific heat of adsorbed hydrogen above the supercritical temperature exhibits the same characteristics as that of compressed hydrogen, so $c_{pa} \approx c_{pg}$. During the adsorption process, molecular interactions between the AC and hydrogen result in energy release, and the increase in the kinetic energy of gas molecules during hydrogen compression process also releases heat. Therefore, the heat source in Eq.(8) consists of two parts: adsorption heat Q and compression work W:

$$Q = -\frac{S_m \Delta H}{M_{H_2}} = \rho_b \frac{\partial n_a}{\partial t} \Delta H \tag{11}$$

$$W = \varepsilon_b \beta_T T \frac{Dp}{Dt} = \beta_T T \left[\varepsilon_b \frac{\partial p}{\partial t} + \left(\vec{v} \cdot \nabla\right) p \right] \tag{12}$$

The viscous dissipation term Φ in Eq.(8) is expressed as:

$$\Phi = \underline{\underline{\tau}} : \nabla \vec{v} = \mu \left[\nabla \vec{v} + \left(\nabla \vec{v}\right) - \frac{2}{3} \left(\nabla \cdot \vec{v}\right) \underline{\underline{I}} \right] : \nabla \vec{v} \tag{13}$$

Where, ΔH represents the isosteric heat of adsorption, (J·mol^{-1})； β_T denotes the volumetric thermal expansion factor, for ideal gas state, β_T takes $1/T$. If the hydrogen in the storage tank is in a low-viscosity flow state, Φ can be ignored.

2.4 Adsorption isotherm model

The isothermal adsorption mathematical model of CAH2 is constructed based on the analysis of experimental data and can accurately describe the adsorption characteristics and process of the adsorbent. The adsorption model established for the AC storage tank in this study uses the modified Dubinin-Astakhov (D-A) model to describe it, and uses the variable isosteric adsorption heat instead of the constant adsorption heat [36]:

$$n_a = n_{\max} \exp\left[-\left(\frac{RT}{\alpha_{D-A} + \beta_{D-A} T} \ln \frac{p_0}{p} \right)^m \right] \tag{14}$$

Where, $n_{\max}$ is the maximum adsorption capacity, (mol·kg^{-1}); R denotes the universal gas constant; For most adsorbents of adsorbed gases, the exponent m usually ranges between 1 and 2. For AC adsorbing hydrogen gas, m takes 2 [36]. p denotes the equilibrium pressure; $\alpha_{\text{D-A}}$ is the enthalpy factor; $\beta_{\text{D-A}}$ is the entropy factor; p_0 is the saturation vapor pressure at T.

According to the chain rule of derivation for composite functions, the mathematical form of the partial derivative of the absolute adsorption capacity n_a of the source term S_m in Eq.(1):

$$\frac{\partial n_a}{\partial t} = m n_a \left(\frac{RT}{\alpha_{D-A} + \beta_{D-A} T} \ln \frac{p_0}{p} \right)^m \left[\frac{1}{\ln(p_0/p)} \frac{1}{p} \frac{\partial p}{\partial t} - \frac{\alpha_{D-A}}{\alpha_{D-A} + \beta_{D-A} T} \frac{1}{T} \frac{\partial T}{\partial t} \right] \tag{15}$$

Hydrogen molecules entering the AC micropores (1~10nm) interact with the AC through van der Waals forces. This interaction force leads to the formation of the adsorbed phase. The heat released during the transition from gas phase to adsorbed phase is called adsorption heat. Based on the modified Dubinin-Astakhov model, the isosteric heat of adsorption is calculated as [36]:

$$\Delta H = -R\left[\frac{\partial(\ln p)}{\partial(1/T)}\right]_n = \alpha_{D-A}\left[\ln\left(\frac{n_{\max}}{n_a}\right)\right]^{1/2} \tag{16}$$

3 Model parameters and verification

3.1 Geometric model

The hydrogen storage tank is a cylindrical container filled with AC, with its outer wall directly in contact with the coolant. The hydrogen inlet is located at the top of the tank, and the total volume is 2.5 L. The axisymmetric geometrical structures of both the conventional hydrogen storage tank and the tank added heat transfer fins are shown in Fig.1 for the computational model. The structural parameters of the tank are as: H_1=0.45m, H_2=0.454m, W_1=0.005m, W_2=0.004m, R_1=0.0508m, R_2=0.469m. The fin structure parameters are adjustable design variables in the following study: L_1=20~45mm; W_3=0.5~3.5mm. To monitor changes in the physical state fields (pressure, temperature, adsorption concentration) inside the hydrogen storage tank, four different detection points are selected in Fig.1: C_1(0, 0.22025), C_2(0, 0.12165), C_3 (0, 0.035), C_4 (0.02345, 0.20525).

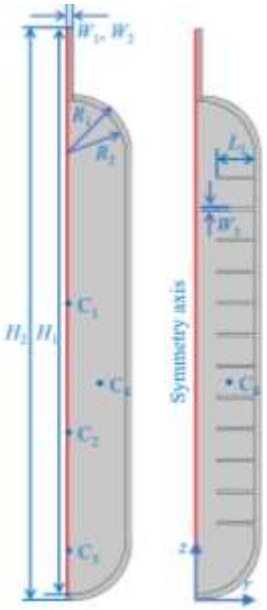

Figure 1. Conventional hydrogen storage tank (left) and storage tank with added heat transfer fins (right)

The geometric model mesh is constructed by the automatic division method based on physical field and multi-field coupling in Comsol Multiphysics. The mesh density selects the Extra-fine mode. The divided mesh of the conventional tank and the tank added fins are depicted in Fig.2, with element counts of 4892 and 6250, respectively. The sensitivity analysis is performed on meshes with different element densities (Finer mesh mode, Extra-fine mesh mode and Extremely-fine mesh mode), and it is found that the mesh density under the Extra-fine scheme can save calculation time while ensuring the accuracy and stability of numerical calculations.

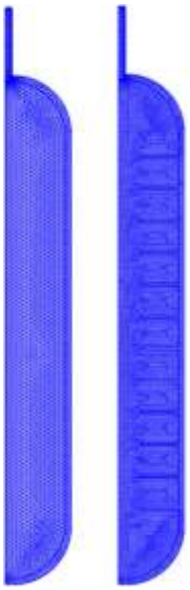

Figure 2. The mesh of the conventional tank (left) and the tank added fins (right)

3.2 Material properties

The shell and fins of the storage tank are made of stainless steel, which is placed in a Dewar flask filled with coolant at a constant temperature of 77K, and with a working pressure below 100 bar. Since 77 K is more than double the critical temperature of hydrogen (33.19 K), and the operating pressure is also far from the critical pressure. In this state, the compressibility factor of hydrogen is close to 1, and hydrogen is in a gaseous state and far from condensation, behaving almost like an ideal gas. Therefore, this study assumes that hydrogen is the ideal gas [37]. The relevant material properties are depicted in Table 1. According to the adsorption characteristics of AC [38], the relevant parameter of the modified Dubinin-Astakov model in Section 2 are obtained by fitting the experimental data [36], as shown in Table 2.

Table 1. Material properties of the calculation model

Properties	Activated carbon	Hydrogen	Steel wall
Bulk density, r_b, kg·m^{-3}	269	Ideal gas	7830
Specific heat, cp, J·kg^{-1}·K^{-1}	825	14700	468
Conductivity, k, W·m^{-1}·K^{-1}	0.764	0.206	13
Bed porosity, ε_b	0.49	—	—
Particle diameter, d_p, mm	2.0	—	—
Dynamic viscosity, μ, Pa·s	—	8.411e-6	—

Table 2. Dubinin-Astakov model parameters for AC

Adsorbents	n_{max}, mol·kg^{-1}	P_0, MPa	$\alpha_{D\text{-}A}$, J·mol^{-1}	$\beta_{D\text{-}A}$, J·mol^{-1}·K^{-1}
Activated carbon	71.6	1470	3080	18.9

3.3 Boundary conditions

As described in our previous study [5], to keep the filling process similar to the one used in the hydrogen refueling station, a variable pressure boundary condition is applied at the tank inlet. As shown in Fig.3, the inlet pressure increases from 0.1 MPa to 10 MPa within 15s, and then remains constant throughout the simulation process. The initial pressure of the tank is 101325 Pa, and the initial temperature is 233 K. The hydrogen flows into the tank at a temperature of 77K. The stainless-steel tank is cooled by a Dewar flask at 77K, so the tank wall temperature is at a constant temperature condition. The filling time is 600s.

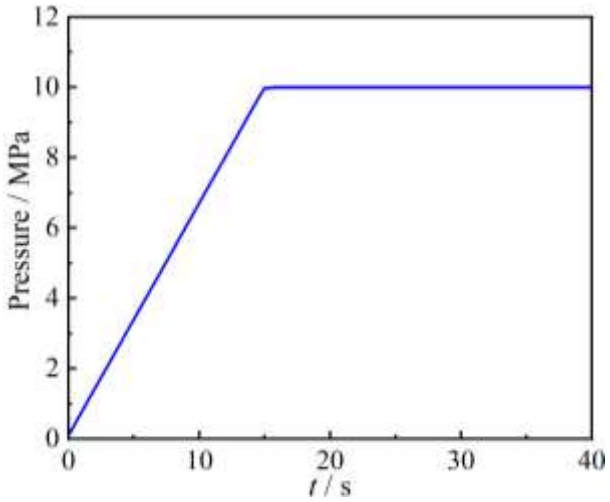

Figure 3. Changes of hydrogen filling pressure at tank inlet with time

3.4 Computational model verification

In order to illustrate the accuracy of the calculation model established above, this study verifies the model based on the AC hydrogen adsorption experiment of Xiao et al [36]. The model validation uses the physical model established above and the same boundary conditions as in the reference experiment. The tank is at 0.03208 MPa and 302 K as initial pressure and initial temperature respectively. The tank wall is imposed the constant temeprature 302.5K. The flow rate of hydrogen entering the tank is 2.048e-05 $kg \cdot s^{-1}$. During the filing process, the variation of the calculated pressure data over time is consistent with the experimental data, as described in Fig.4. The calculated temperature at points C_1 and C_2 over time compared with the experimental data are as depicted in Fig.5(a) and Fig.5(b). The numerical results tend to underestimate the experimental results, but generally maintain good consistency.

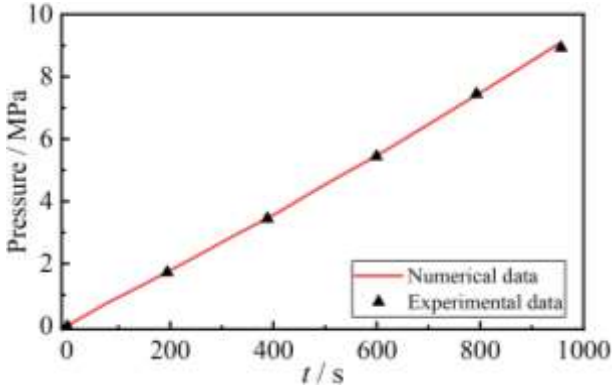

Figure 4. Pressure comparison between the numerical and the experimental during filling

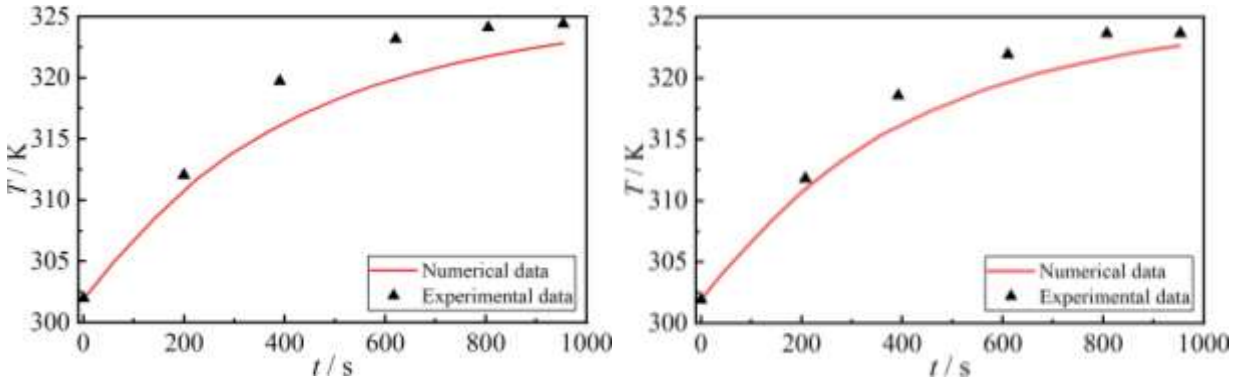

(a) C_1 (2) C_2

Figure 5. Temperature comparison between the numerical and the experimental during filling at selected locations

4. Result and discussions

Previous studies [26,35] have shown that the adsorption heat and the compression work generated during the adsorption process cause the overall temperature in the tank to rise. Excessive heat accumulation in specific regions will lead to local high temperature. Excessive overall temperature seriously reduces the hydrogen adsorption rate and storage capacity, and also increases the internal pressure of the storage tank, raising system safety risks. Local high temperature can cause the desorption of already adsorbed hydrogen, further reducing storage efficiency. According to Le Chatelier's principle, local high temperature shifts the adsorption equilibrium in a direction unfavorable to adsorption, decreasing the adsorption amount. Moreover, prolonged local high temperatures can degrade the structure of the AC in those areas, reducing its adsorption capacity and stability. Therefore, effective thermal management measures are essential to lower the average temperature and suppress local overheating. Considering the effective application of high thermal conductivity metal fins in other thermal management devices, and no research has yet explored the gain effect of fins on the CAH2 tank; this study is the first to explore the effectiveness of adding fins to the inner wall of the storage tank for thermal management and its impact on hydrogen storage performance. The influence mechanism of fin arrangement, fin number (spacing), fin width and fin length on hydrogen storage efficiency and temperature field is comprehensively analyzed.

4.1 Effect of fin arrangement on adsorption process

4.1.1 Fin arrangement schemes

Based on the same fin surface area, fin number, fin length and fin width, three different fin design schemes within the tank are considered: conventional no-fin scheme, inclined fin scheme, and bottom fin scheme. The structure comparison of the no-fin tank and the three added fin tanks is shown in Fig.6.

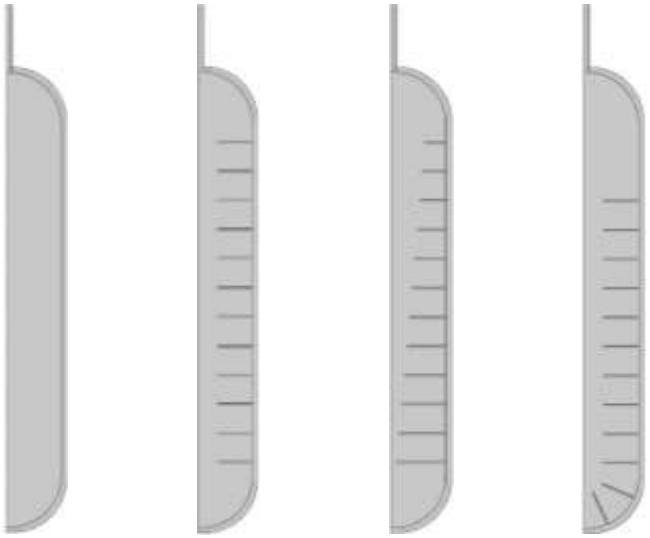

(a) No-fin (b) Conventional fin (c) Inclined fin (d) Bottom fin

Figure 6. Hydrogen storage tank without fins and with fins in three different arrangements

4.1.2 Result analysis

Fig.7 shows the distribution of the temperature field and the absolute adsorption concentration field of hydrogen at different times under various fin arrangement schemes. It can be noted that the lower the temperature, the higher the absorption concentration of hydrogen, and the adsorption concentration distribution highly corresponds with the temperature distribution. As filling time progresses, the local high-temperature regions and local low adsorption concentration regions decrease in all four schemes. However, the large high heat region concentrated in the center of the no-fin tank diffuses more slowly, and the timely transfer of this part of heat will greatly increase the adsorption amount. At the same filling time, the local high-temperature area and maximum temperature value of the three fin schemes are significantly lower than that of the no-fin scheme. Similarly, the local low adsorption concentration regions of the three fin schemes are noticeably smaller, and the minimum adsorption concentration values are higher than that of the no-fin scheme. Although in the initial stage of hydrogen filling (t=100s), some small mid-temperature regions exist between the top fins due to the hindrance of heat convection of low-temperature incoming hydrogen by the top fins, weakening hydrogen adsorption in these regions, as time progresses (t=300s and t=500s), the heat conduction effect of the low-temperature fins strengthens, eliminating these mid-temperature regions between the top fins. In general, adding fins significantly enhances heat dissipation within the storage tank and increases adsorption concentration. The temperature field and adsorption concentration field distribution under different fin schemes are different, but there are obvious small-scale high-temperature regions at the bottom and around the bottom fins of the tank. This is because the adsorption heat first generated by the adsorption reaction near the inlet will flow with the hydrogen to the vicinity of the bottom and generate heat accumulation, and the accumulation of hydrogen pressure at the bottom will also generate compression heat. The bottom-fin scheme enhances heat conduction around the bottom area, causing the high-temperature region to move upward without reducing its area. At t=100s, the local high-temperature region at the bottom is largest in the bottom-fin scheme and smallest in the inclined-fin scheme. However, at t=300s and t=500s, as heat conduction effect becomes dominant, the conventional fin scheme shows the largest local high-temperature region at the bottom, while the bottom-fin scheme shows the smallest. Therefore, in the early stages of filling, the inclined-fin scheme exhibits the best heat dissipation and adsorption effects, while in the mid-to-late stages of filling, the bottom-fin scheme performs best in heat dissipation and adsorption.

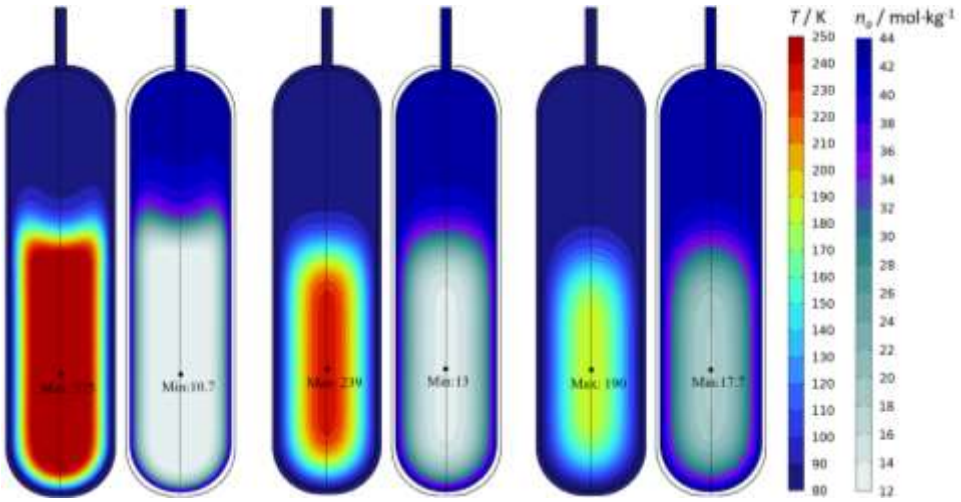

(a) 100s (b) 300s (c) 500s

(a) No-fin tank

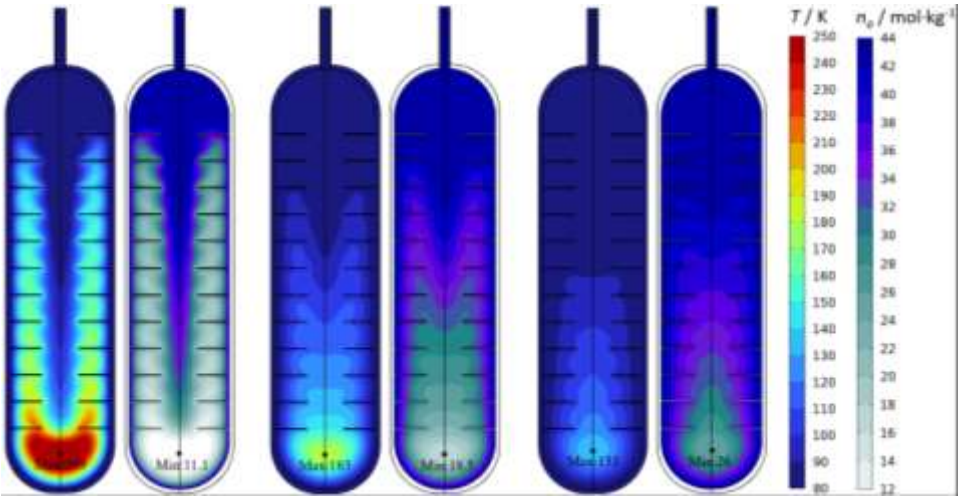

(a) 100s (b) 300s (c) 500s

(b) Conventional fin tank

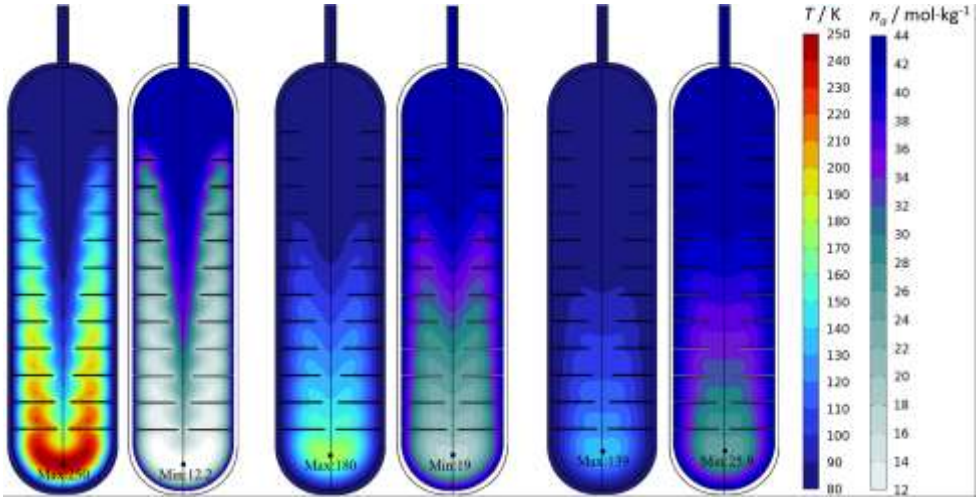

(a) 100s (b) 300s (c) 500s

(c) Inclined fin tank

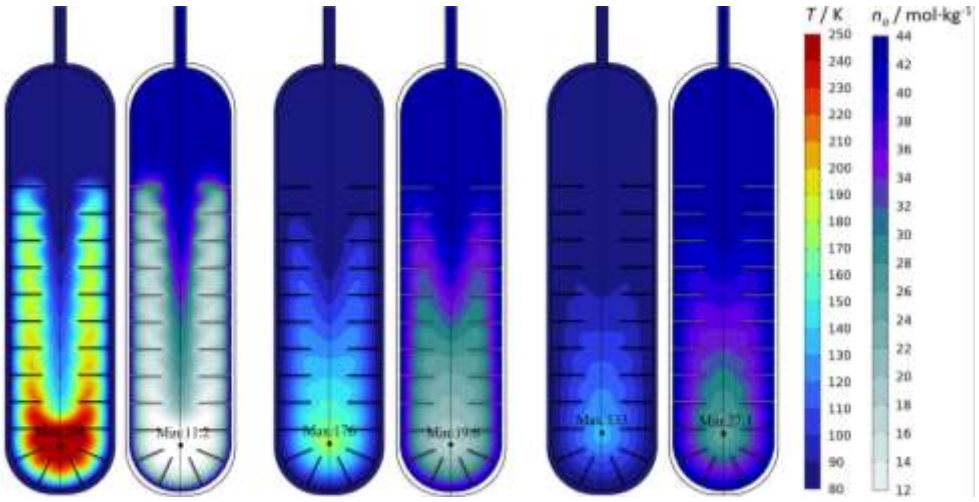

(a) 100s (b) 300s (c) 500s

(d) Bottom fin tank

Figure 7. Temperature field and absolute adsorption concentration field of hydrogen at different times under different fin schemes

The average temperature and total adsorption amount of the tank can reflect the overall heat exchange effectiveness and hydrogen storage efficiency. Fig.8 and Fig.9 show the changes in average temperature and adsorption amount during the filling process for different tank schemes, respectively. At the beginning of filling, the AC adsorbs a large amount of hydrogen and releases significant heat, resulting in a high internal temperature. With the inflow of low-temperature hydrogen and the cooling of the low-temperature wall, the average temperature gradually decreases. Throughout the filling process, the average temperature of the three fin schemes is significantly lower than that of the no-fin scheme, and the temperature reduction rate is noticeably faster. The temperature trends of the three fin schemes are almost identical, indicating that changes in fin arrangement have minimal impact on the overall average temperature when the fin area, number, width, and length are the same. Similarly, the adsorption amount curves over time for the three fin schemes are nearly identical. In the initial stage of filling, the temperature of the bottom fin scheme is higher than the other two fin schemes. However, in the mid-to-late stages of filling, the temperature of the bottom fin scheme is lower than the other two fin schemes. In the first 50s, the adsorption amount of the no-fin scheme is slightly higher than that of the three fin schemes. After 50s, the adsorption rate of the three fin schemes accelerates, with adsorption amount significantly exceeding that of the no-fin scheme. When the adsorption amount reaches 0.05 kg, the times required for the no-fin scheme, conventional fin scheme, inclined fin scheme, and bottom fin scheme are 560s, 342s, 337s, and 331s, respectively. Among them, the bottom fin scheme has the highest storage rate, reducing the filling time by 41% compared to the no-fin scheme.

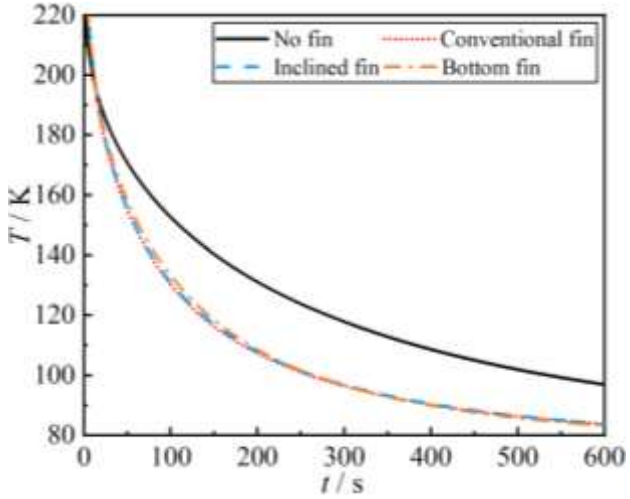

Figure 8. Overall average temperature variation over time for different fin arrangement schemes

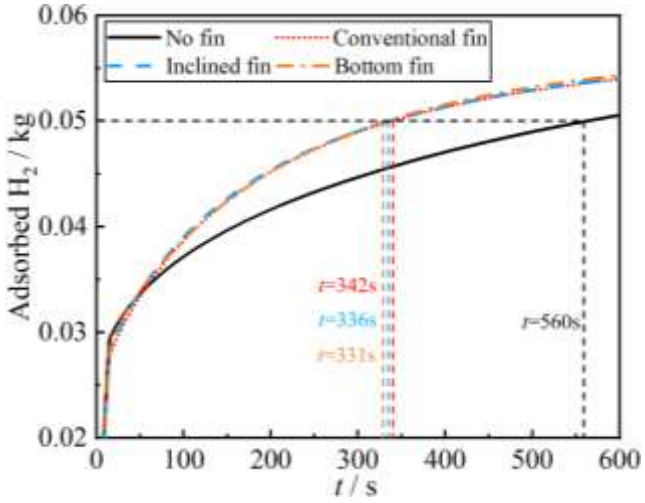

Figure 9. Adsorption amount variation over time for different fin arrangement schemes

Long-term local high temperature inside the tank will affect the adsorption equilibrium and render the AC structure ineffective, reducing its adsorption capacity and stability, as well as its lifespan over multiple inflation and deflation cycles. Fig.10 and Fig.11 show the changes in maximum temperature T_{max} and minimum adsorption concentration $n_{\text{a-min}}$ over time for different tank schemes. The physical field distributions in Fig.7 indicate that T_{max} and $n_{\text{a-min}}$ occur at the same location, so the trend of $n_{\text{a-min}}$ changes correspondingly with T_{max}. As the inflation time t increases, the T_{max} curve gradually decreases, and the $n_{\text{a-min}}$ curve gradually increases. The T_{max} and $n_{\text{a-min}}$ curves for the three fin schemes change more rapidly than those for the no-fin scheme. In the early stages of filling, the no-fin scheme exhibits the highest and longest-lasting T_{max}, the inclined fin scheme shows the lowest and shortest-lasting T_{max}. Among three fin schemes, the T_{max} of the conventional fin scheme is the highest and lasts the longest, so its $n_{\text{a-min}}$ is the lowest and lasts the longest.

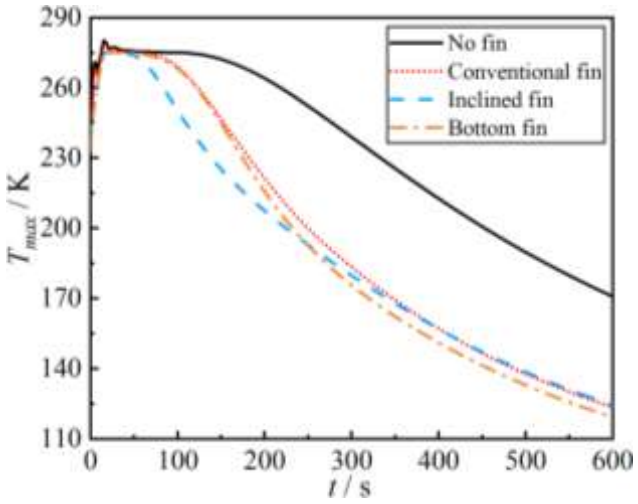

Figure 10. Changes of maximum temperature T_{max} inside the storage tank over time under different fin arrangement schemes

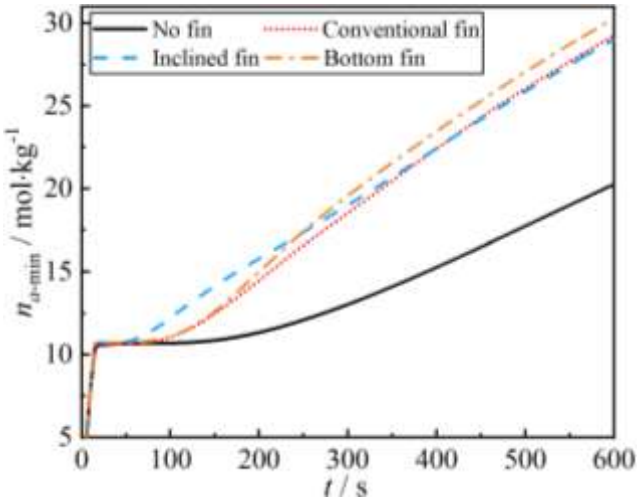

Figure 11. Changes of the minimum absolute adsorption concentration $n_{a\text{-}min}$ inside the storage tank over time under different fin arrangement schemes

Fig.12 shows the temperature change of the above fin schemes at different detection points (C_1, C_2, C_3, C_r) over time. As filling time progresses, the temperatures at all detection points exhibit a trend of first increasing and then decreasing. The temperature change of the no-fin scheme along the hydrogen flow direction (from C_1 through C_2 to C_3) is first increasing and then decreasing. This is due to the local high temperature region of the no-fin tank is concentrated in a large area of the tank center (near point C_2), while point C_1 is affected by the low-temperature inflow hydrogen at the inlet, and point C_3 is affected by the low-temperature wall at the bottom, both with lower temperature. Conversely, the temperature of the three fin schemes along the hydrogen flow direction is gradually increased. Due to the heat conduction enhancement effect of fins, the temperatures of the three fin schemes at the four detection points are all lower than that of the no-fin scheme. The temperature difference between the fin schemes and the no-fin scheme is largest at C_1 and C_2, and smallest at C_3, indicating that the fins are less effective at cooling the bottom of the tank. At C_2, the temperatures in the three fin schemes fluctuate due to the heat transfer from high-temperature hydrogen between the fins to the center and the shift in adsorption equilibrium at high temperatures. At C_1, the cooling effect of the three fin schemes is similar. At C_r and C_2, the conventional fin scheme provides the best cooling effect, whereas at C_3, the bottom fin scheme is most effective. This is because the inclined fin scheme impedes the heat convection transport of low-temperature hydrogen at the rear of the tank, while the bottom fin tends to enhance the heat conduction at the bottom of the tank.

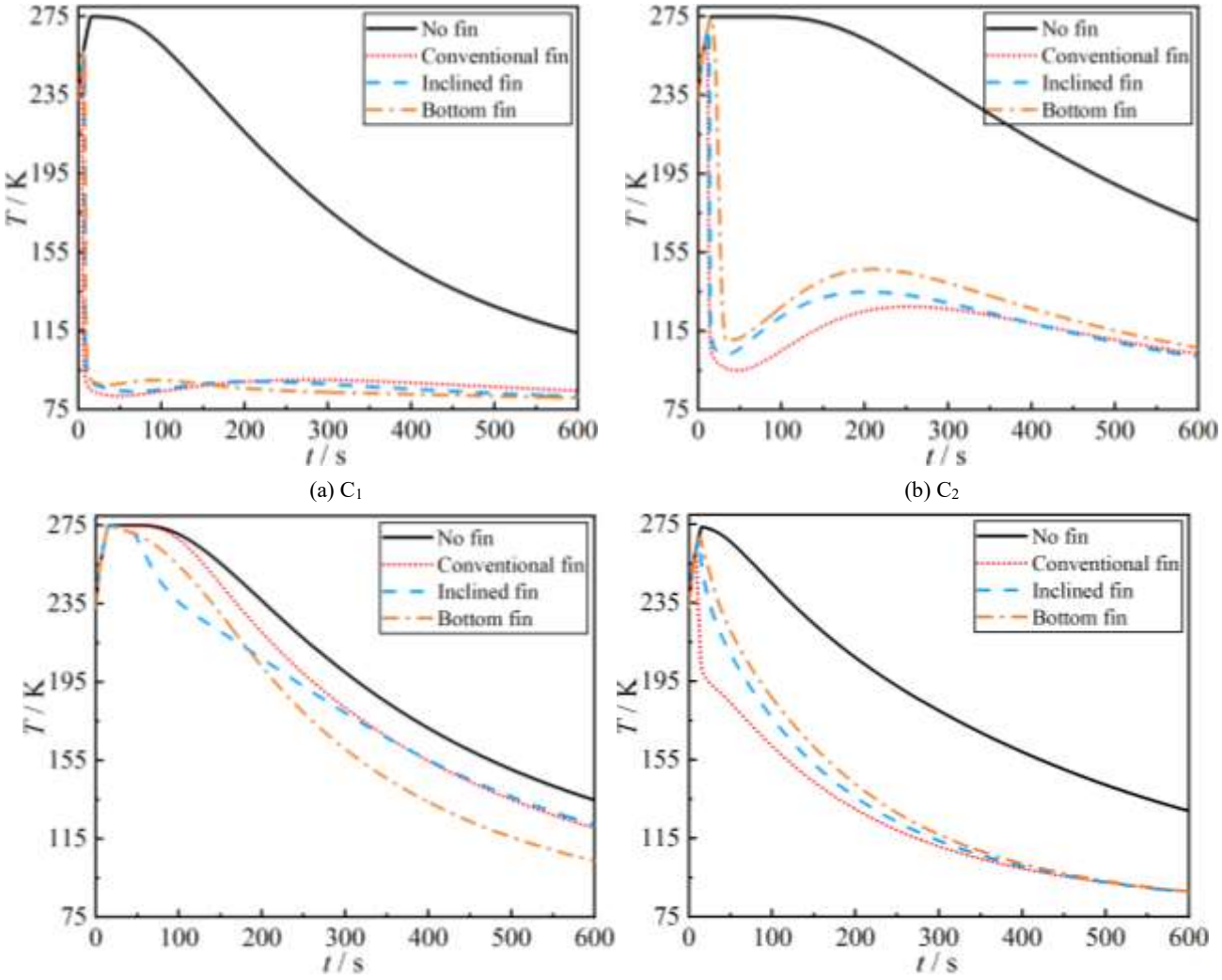

(a) C_1 (b) C_2

(c) C_3 (d) C_r

Figure 12. Temperature variation over time at different detection points (C_1, C_2, C_3, C_r) for four fin schemes

4.2 Effect of fin length on adsorption process

4.2.1 Fin length schemes

Based on the conventional fin scheme in Section 4.1, with the same number of fins, fin spacing and fin width as the design principle, six different fin length schemes (20mm, 25mm, 30mm, 35mm, 40mm, 45mm) are designed. The fin structures under six different lengths can be referred to Fig.13.

4.2.2 Result analysis

Fig.13 shows the internal temperature and adsorption concentration distribution of the storage tank at t=200s for different fin length schemes. As the fin length increases (from 20mm to 40mm), the high temperature area at the bottom of tank gradually reduces, and the maximum temperature within this area also decreases. Correspondingly, the low adsorption concentration area gradually reduces, and the minimum adsorption concentration value within this area increases. However, the reduction rate of the high-temperature area and the low adsorption concentration area is significantly reduced. When the fin length increases from 40mm to 43mm, both the high-temperature area and the low adsorption concentration area start to rebound and increase. Therefore, longer fins do not necessarily result in better heat dissipation effect. This phenomenon can be attributed to the primary heat transfer mechanisms within the tank, which include convection transfer between low-temperature and high-temperature hydrogen, and thermal

conduction between the fins and high-temperature regions. The Length=43mm fin obstructs the flow of cold hydrogen into the tank bottom, weakening the convection heat transfer effect between the cold and hot hydrogen in this region. Additionally, shorter fins result in smaller mid-temperature regions formed between the fins near the tank top, but longer fins do not offer an advantage in heat dissipation for this region. This is because the convection heat transfer caused by cold inflow hydrogen at the tank top plays a dominant role, and the semi-enclosed regions formed by longer fins hinder the entry of cold hydrogen, leading to relatively larger mid-temperature regions. As the fin length increases, this temperature characteristic becomes more pronounced. However, with the increase in filling time, the heat conduction effect of the low-temperature fins and the diffusion effect of the cold hydrogen strengthen, causing these mid-temperature regions to gradually disappear. Therefore, there exists an optimal fin length range that maximizes the overall heat transfer efficiency within the tank.

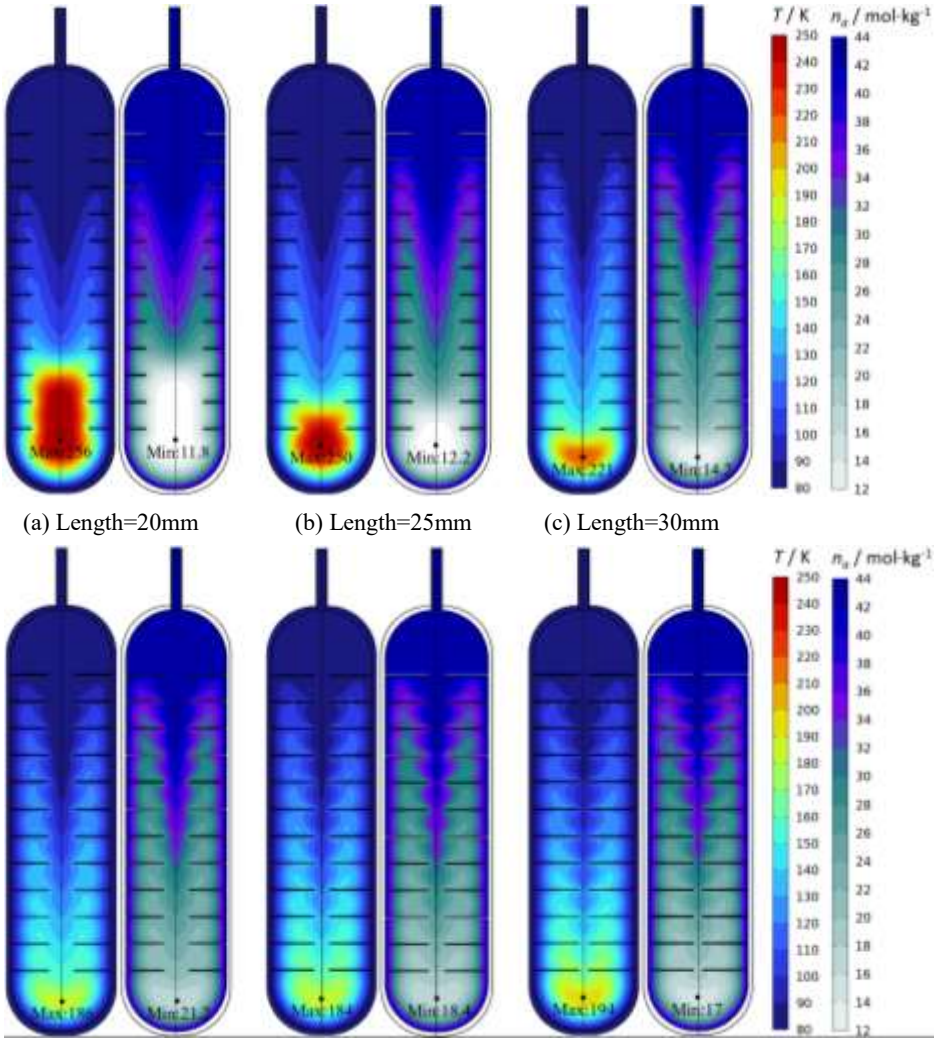

(a) Length=20mm (b) Length=25mm (c) Length=30mm

(d) Length=35mm (e) Length=40mm (f) Length=45mm

Figure 13. Temperature field and absolute adsorption concentration field of hydrogen at different fin length schemes at t=200s

The changes of overall average temperature and total adsorption amount with time under different fin length schemes are shown in Fig.14 and Fig.15, respectively. As the filling time increases, the average temperature inside the tank gradually decreases, and the adsorbed hydrogen amount gradually increases. In the initial stage of filling, the adsorption reaction is not intense, and the heat conduction effect of the fins is weak, resulting in minimal temperature differences among the six schemes. After t>100s, the differences in heat conduction and convection effects among the fin schemes become apparent, leading to significant variations in the temperature curves. The

Length=30mm scheme exhibits the lowest temperature, indicating that its internal heat conduction and convection effects achieve an optimal balance, thus maximizing the overall heat and mass transfer process. The temperature curves of the Length=25mm and Length=35mm schemes are close to that of the Length=30mm, also demonstrating good heat transfer performance. The temperature of Length=45mm scheme is the highest, followed by Length =20mm, because these two have very poor convective heat transfer and heat conduction effects respectively. The change curves of adsorption amount indicate that, except for the 20mm fin scheme, the change characteristics of the adsorption amount with the fin length of the other schemes correspond to their temperature curves. The Length=30mm scheme has the highest adsorption amount, followed by the Length=25mm, while the Length=45mm scheme has the lowest adsorption amount. When the adsorption amount reaches 0.05kg, the time required for Length=30mm scheme is 13% less than that for the Length=25mm. Since the fin volume of Length=20mm scheme is the smallest, it indirectly increases the hydrogen capacity of the tank. Therefore, although the temperature inside is very high, its adsorption amount is not very low.

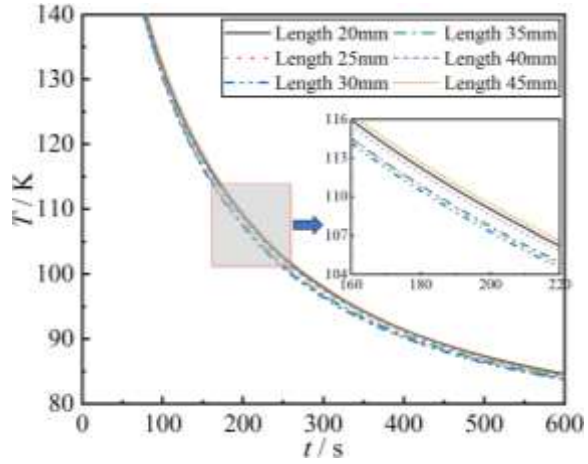

Figure 14. Overall average temperature variation over time for different fin length schemes

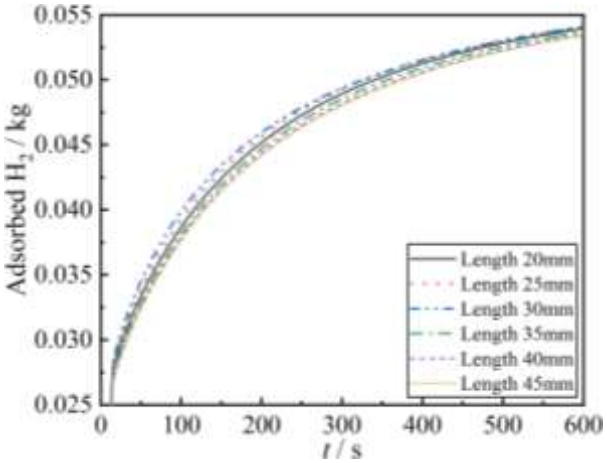

Figure 15. Total adsorption amount variation over time for different fin length schemes

4.3 Effect of fin number on adsorption process

4.3.1 Fin number schemes

Based on the conventional fin in Section 4.1, and with the same fin length and fin width as the design principle, six different fin number schemes (8, 10, 12, 14, 16, 18) are designed. Different fin numbers imply different spacing between fins, where increasing the number of fins decreases the spacing between them. The tank structure with six different fin numbers can be found in Fig.16.

4.3.2 Result analysis

Fig.16 shows the temperature and adsorption concentration distributions within the storage tank at t=200s for different fin number schemes. At t=200s, different fin number schemes all exhibit local mid-temperature regions between the fins in the middle and upper parts of the tank, as well as local high-temperature regions at the bottom of the tank. Correspondingly, local regions of medium adsorption concentration and low adsorption concentration appear in the same positions as these mid-temperature and high-temperature regions. As the number of fins increases, the positions of these local mid-temperature and high-temperature regions remain unchanged, but the areas and maximum temperature values of these regions decrease significantly. Similarly, the minimum concentration value of the local low concentration region increases with the number of fins, and the area of these low concentration region decreases. This indicates that increasing the number of fins significantly enhances the heat and mass transfer during the adsorption process, thereby effectively promoting hydrogen adsorption.

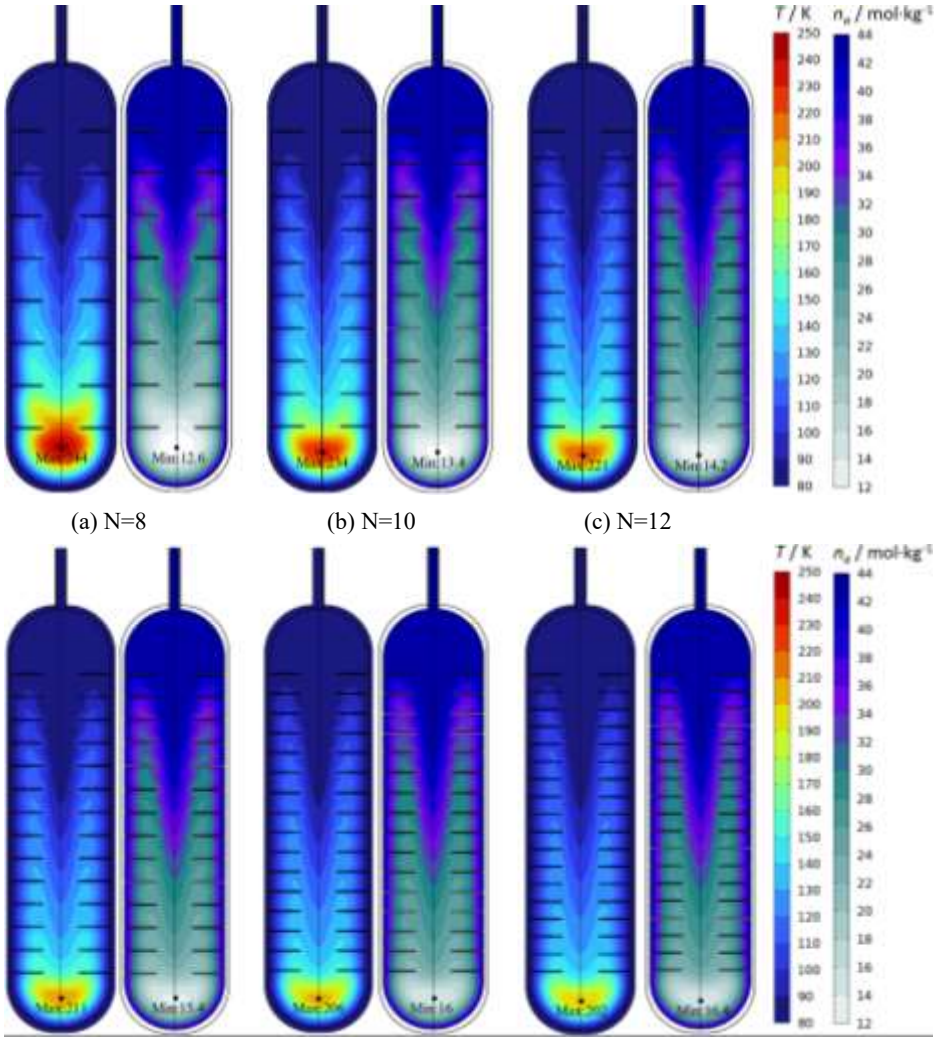

(a) N=8 (b) N=10 (c) N=12

(d) N=14 (e) N=16 (f) N=18

Figure 16. Temperature field and absolute adsorption concentration field of hydrogen at different fin number schemes at t=200s

The changes of overall average temperature and total adsorption amount with time under different fin number schemes are shown in Fig.17 and Fig.18, respectively. In the initial stage of filling, the temperature and adsorption amount curves for different fin number schemes show little difference. After t>100s, the differences in temperature and adsorption amount among the various schemes become apparent and gradually increase. With the increase of fin number, the average temperature decreases, and the adsorption amount increases, consistent with the temperature and adsorption concentration distributions shown in Fig.16. Thus, more fins achieve better heat transfer effect, resulting

in higher adsorption amount. And a high number of fins can overcome the disadvantage of reduced tank volume to increase the adsorption amount compared to a low number of fins. The average temperature of N=18 scheme is the lowest and its adsorption amount is the highest, followed by N=16; the average temperature of N=8 is the highest and its adsorption amount is the lowest. When the adsorption amount reaches 0.05kg, the time spent on filling of N=18 scheme is reduced by 9.4% relative to N=8 scheme. However, as the fin number increases, the change rate of in temperature and adsorption amount decreases significantly. From Fig.19 and Fig.20, the changes in average temperature and adsorption amount at t=300s show that the change rate of for both curves begins to slow after the fin number exceeds 14. After N>14, the gain effect brought about by further increasing the fin numbers diminishes noticeably. Therefore, the N=14 is a relatively optimal choice, achieving relatively better performance at a relatively small fin cost.

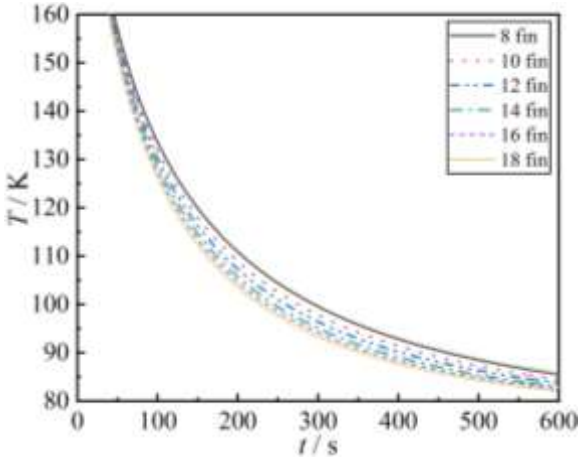

Figure 17. Overall average temperature variation over time for different fin number schemes

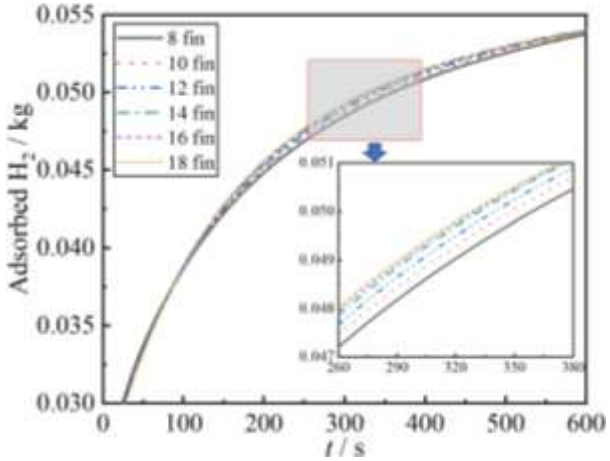

Figure 18. Total adsorption amount variation over time for different fin number schemes

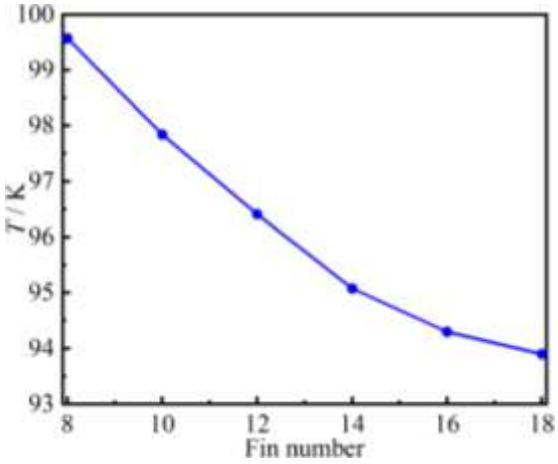

Figure 19. Average temperature variation over fin number at *t*=300s

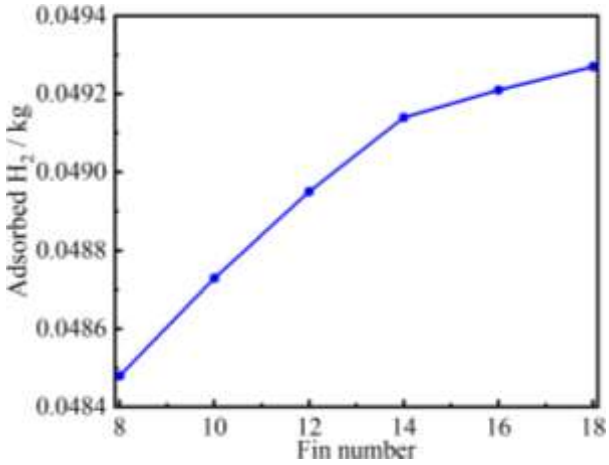

Figure 20. Adsorption amount variation over fin number at *t*=300s

4.4 Effect of fin width on adsorption process

4.4.1 Fin width schemes

Based on the conventional fin scheme in Section 4.1, with the same number of fins and fin length as the design principle, six different fin width schemes (0.5mm, 1mm, 1.5mm, 2.0mm, 2.5mm, 3.5mm) are designed. The fin structures under six different widths can be referred to Fig.21.

4.4.2 Result analysis

Fig.21 shows the temperature field and adsorption concentration field within the storage tank at *t*=200s for different fin width schemes. Different fin widths have almost no effect on the position of the mid-temperature regions in the middle and top of tanks and the high-temperature region at the bottom of tanks, only affecting their area and temperature value. This is because increasing the fin width does not exponentially increase the heat transfer area like increasing the fin length and number does, and its effect on heat conduction and convection is also weaker. As the fin width increases, the area and maximum value of the high-temperature region decrease, but the reduction amplitude is not substantial. Correspondingly, the adsorption concentration field exhibits similar change characteristics with increasing fin width.

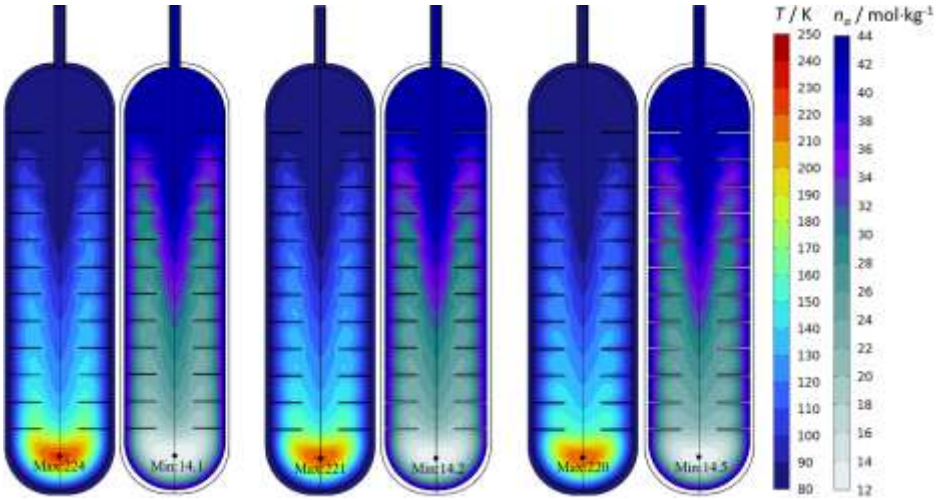

(a) Width=0.5mm (b) Width=1mm (c) Width=1.5mm

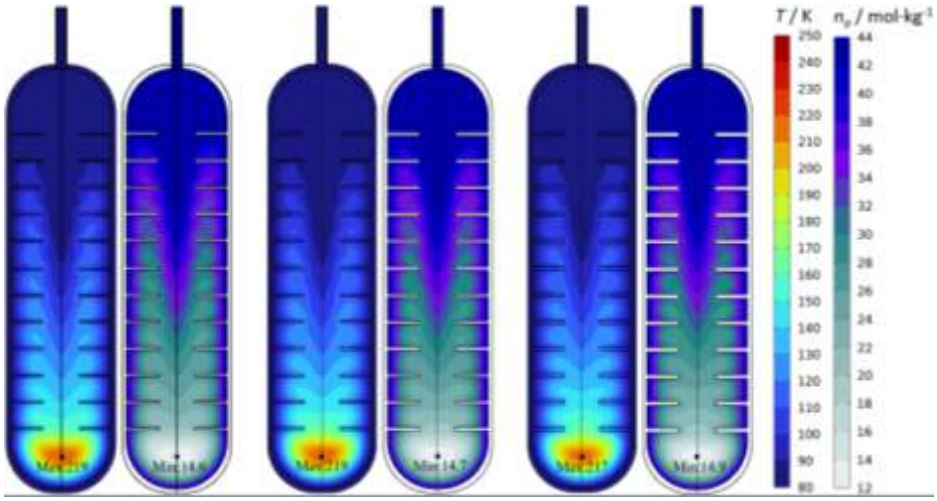

(d) Width=2.0mm (e) Width=2.5mm (f) Width=3.5mm

Figure 21. Temperature field and absolute adsorption concentration field of hydrogen at different fin width schemes at t=200s

The changes of overall average temperature and total adsorption amount with time under different width schemes are shown in Fig.22 and Fig.23, respectively. As the fin width increases, the average temperature inside the tank gradually decreases. After t>100s, the temperature differences between the different fin width schemes become more pronounced with increasing filling time. The Width=3.5mm scheme achieves the lowest overall average temperature, while the Width=0.5mm scheme has the highest average temperature. However, the adsorption amount does not exhibit the same variation trend with increasing fin width as the temperature does, and it decreases with increasing fin width. The Width=3.5mm scheme has the lowest adsorption amount, whereas the Width=1.0mm scheme achieves the highest adsorption amount, followed by Width=0.5mm. This discrepancy arises because the total adsorption amount is influenced not only by temperature condition but also by the tank volume. Although Width=3.5mm provides the lowest temperature conditions for the adsorption reaction, its fin volume is 3.5 times and 7 times larger than that of Width=1.0mm and Width=0.5mm, respectively, thus significantly reducing the hydrogen storage space. When the adsorption amount reaches 0.05kg, the charging time for Width=1.0mm scheme is reduced by 25% compared to Width=3.5mm scheme. Therefore, although increasing the fin width is beneficial to reducing the average temperature of storage tank, it will have a negative effect on the total storage capacity and storage efficiency. Under the premise of comprehensively considering the overall temperature, adsorption efficiency and total hydrogen storage amount, it is more reasonable to adopt the solution of Width=1.0mm.

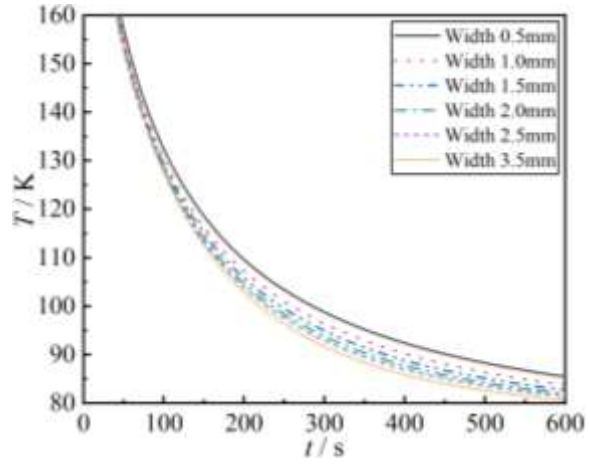

Figure 22. Overall average temperature variation over time for different fin width schemes

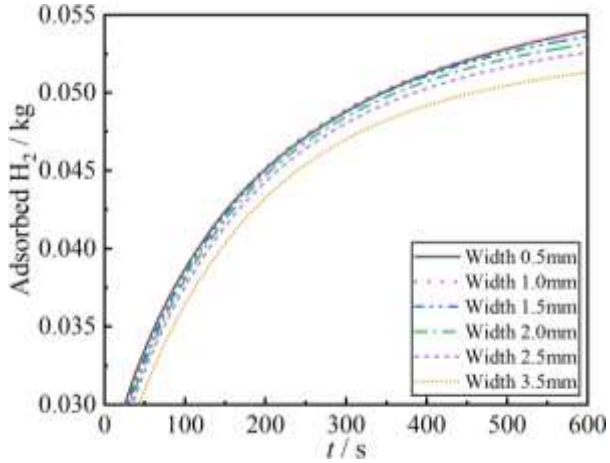

Figure 23. Total adsorption amount variation over time for different fin width schemes

5. Conclusions

This study establishes a numerical model for the CAH2 using activated carbon storage tank. The physical reasons for the local high temperature accumulation and low adsorption efficiency of traditional hydrogen storage tanks are analyzed. Adding high thermal conductivity fins is innovatively proposed to enhance the heat and mass transfer, thereby improving the adsorption efficiency and storage amount. The effects of different fin arrangement schemes, fin lengths, fin numbers and fin widths on the hydrogen adsorption process are investigated. The main conclusions are as follows:

(1) The heat effect of the adsorption process is a major obstacle affecting the adsorption efficiency and storage amount. Adding fins efficiently conducts the adsorption heat and compression work generated by the adsorption reaction compared to traditional finless tanks, significantly reduce the area and maximum temperature of the local high-temperature regions, and thus promote the overall adsorption equilibrium, increasing the global hydrogen adsorption rate and storage amount.

(2) The heat and mass transfer during the adsorption process is influenced by both heat conduction and heat convection transfer. Different fin arrangement schemes have significantly different effects on local temperature and adsorption concentration fields, but have little effect on the overall average temperature and total adsorption amount, and also have different effects on different filling stages. Overall, the bottom-fin scheme has the highest storage efficiency. When the adsorption amount reaches 0.05 kg, the filling times for the bottom-fin, inclined-fin, and conventional-fin schemes are reduced by 41%, 39.8%, and 38.9%, respectively, compared to the no-fin scheme.

(3) Increasing the fin length enhances the thermal conduction effect, but longer fins can weaken the heat convective transfer effect. The heat conduction and convection effects in the tank with Length=30mm fins have reached an effective balance to maximize the entire heat and mass transfer process, so its overall temperature is the lowest, and the adsorption rate and storage amount are the highest. The severe inhibition of heat convective transfer by Length=45mm fins results in the highest overall temperature and the lowest adsorption amount.

(4) Different fin numbers have little impact on the distribution position of local high-temperature and low adsorption concentration regions, but significantly affect the area and variable extremum of these regions. More fins are conducive to enhancing the heat and mass transfer process and promoting the adsorption reaction. However, after fin number exceeds 14, the gain effect of increasing fin number on enhancing heat transfer and storage efficiency begins to weaken significantly.

(5) The change in fin width has the weakest effect on the temperature field and adsorption concentration field compared with the fin length and fin number. Although increasing fin width reduces the area and extremum of local high-temperature and low-concentration regions, the reduction amplitude is minimal. Since increasing the fin width greatly reduces the effective tank volume, the changing of the global average temperature with the increase in fin width is opposite to the total adsorption amount. The large fin width (Width=3.5mm) has the lowest overall temperature, its adsorption amount is also the lowest. Under the premise of comprehensively considering the overall temperature condition, adsorption efficiency and amount, Width=1.0mm is more reasonable.

Acknowledgement

MAST3RBoost is a funded by the European Union. Views and opinions expressed are however those of the author(s) only and do not necessarily reflect those of the European Union or the European Health and Digital Executive Agency. Neither the European Union nor the granting authority can be held responsible for them

References

[1] Rasul MG, Hazrat MA, Sattar MA, et al. The future of hydrogen: Challenges on production, storage and applications. Energ Convers Manage 2022; 272: 116326.

[2] Bosu S, Rajamohan N. Recent advancements in hydrogen storage-Comparative review on methods, operating conditions and challenges. Int J Hydrogen Energ 2024; 52: 352-370.

[3] Li H, Cao X, Liu Y, et al. Safety of hydrogen storage and transportation: An overview on mechanisms, techniques, and challenges. Energy Rep 2022; 8: 6258-6269.

[4] Usman MR. Hydrogen storage methods: Review and current status. Renew Sust Energ Rev 2022; 167: 112743.

[5] Melideo D, Ferrari L, Pardelli PT. Preliminary analysis of refilling cold-adsorbed hydrogen tanks. J Phys Conf Seri 2023; 2648(1): 012042.

[6] Zheng J, Liu X, Xu P, et al. Development of high pressure gaseous hydrogen storage technologies. Int J Hydrogen Energ 2012; 37(1): 1048-1057.

[7] Bosu S, Rajamohan N. Recent advancements in hydrogen storage-Comparative review on methods, operating conditions and challenges. Int J Hydrogen Energ 2024; 52: 352-370.

[8] Chen Z, Ma Z, Zheng J, et al. Perspectives and challenges of hydrogen storage in solid-state hydrides. Chinese J Chem Eng 2021; 29: 1-12.

[9] Tao J, Rappe AM. Physical adsorption: Theory of van der Waals Interactions between particles and clean surfaces. Phys Rev Lett 2014; 112(10): 106101.
[10] Xiao J, Peng R, Cossement D, et al. CFD model for charge and discharge cycle of adsorptive hydrogen storage on activated carbon. Int J Hydrogen Energ 2013; 38(3): 1450-1459.
[11] Sdanghi G, Schaefer S, Maranzana G, et al. Application of the modified Dubinin Astakhov equation for a better understanding of high-pressure hydrogen adsorption on activated carbons. Int J Hydrogen Energ 2020; 45: 25912-26.
[12] Melideo D, Ferrari L, Taddei P. Computational Fluid Dynamic (CFD) analysis of a cold-Adsorbed hydrogen tank during refilling. ICHS2023 2023; 09-21.
[13] Yang D, Liang L, Zhang H, et al. Numerical simulation of the hydrogen charging process in an adsorption storage tank. Int J Hydrogen Energ 2024; 68: 673-687.
[14] Hynek S, Fuller W, Bentley J. Hydrogen storage by carbon sorption. Int J Hydrogen Energ 1997; 22(6): 601-610.
[15] Dillon AC, Jones KM, Bekkedahl TA, et al. Storage of hydrogen in single-walled carbon nanotubes. Nature 1997; 386(6623): 377-379.
[16] Peng C, Liu X, Liu Z, et al. Performance optimization of adsorption hydrogen storage system via computation fluid dynamics and machine learning. Chem Eng Res Des 2024; 207: 100-109.
[17] Zhang H, Fu X, Yin J, et al. The effect of MWNTs with different diameters on the electrochemical hydrogen storage capability. Phys Lett A 2005; 339(3-5): 370-377.
[18] Jorda-Beneyto M, Suárez-García F, Lozano-Castello D, et al. Hydrogen storage on chemically activated carbons and carbon nanomaterials at high pressures. Carbon 2007; 45(2): 293-303.
[19] Attia NF, Jung M, Park J, et al. Facile synthesis of hybrid porous composites and its porous carbon for enhanced H2 and CH4 storage. Int J Hydrogen Energ 2020; 45(57): 32797-32807.
[20] Wang L, Wang L, Zhao J, et al. Adsorption of selected gases on metal-organic frameworks and covalent organic frameworks: A comparative grand canonical Monte Carlo simulation. J Appl Phys 2012; 111:112628.
[21] Furukawa H, Miller MA, Yaghi OM. Independent verification of the saturation hydrogen uptake in MOF-177 and establishment of a benchmark for hydrogen adsorption in metal-organic frameworks. J Mater Chem 2007; 17(30): 3197-3204.
[22] Hermosilla-Lara G, Momen G, Marty PH, Le Neindre B, Hassouni K. Hydrogen storage by adsorption on activated carbon: investigation of the thermal effects during the charging process. Int J Hydrogen Energy 2007; 32:1542-53.
[23] Momen G, Hermosilla G, Michau A, et al. Experimental and numerical investigation of the thermal effects during hydrogen charging in packed bed storage tank. Int J Heat Mass Transfer 2009; 52: 1495-1503.
[24] Momen G, Jafari R, Hassouni K. On the effect of process temperature on the performance of activated carbon bed hydrogen storage tank. Int J Therm Sci 2010; 49(8): 1468-1476.
[25] Xiao J, Li Q, Cossement D, et al. Lumped parameter simulation for charge-discharge cycle of cryo-adsorptive hydrogen storage system. Int J Hydrogen Energ 2012; 37(18): 13400-13408.
[26] Xiao J, Liu Y, Wang J, et al. Finite element simulation of heat and mass transfer in activated carbon hydrogen storage tank. Int J Hydrogen Energ 2012; 55(23-24): 6864-6872.
[27] Hou XX, Sulic M, Ortmann JP, et al. Experimental and numerical investigation of the cryogenic hydrogen storage processes over MOF-5. Int J Hydrogen Energ 2016; 41(6): 4026-4038.
[28] Schlemminger C, Næss E, Bünger U. Cryogenic adsorption hydrogen storage with enhanced heat distribution-An in-depth investigation. Int J Hydrogen Energ 2016; 41(21): 8900-8916.
[29] Ubaid S, Zacharia R, Xiao J, et al. Effect of flowthrough cooling heat removal on the performances of MOF-5 cryo-adsorptive hydrogen reservoir for bulk storage applications. Int J Hydrogen Energ 2015; 40(30): 9314-9325.
[30] Liu D, Purewal JJ, Yang J, et al. MOF-5 composites exhibiting improved thermal conductivity. Int J Hydrogen Energ 2012; 37(7): 6109-6117.
[31] Tong L, Xiao J, Cai Y, et al. Thermal effect and flow-through cooling of an adsorptive hydrogen delivery tank. Int J Hydrogen Energ

2016; 41(36): 16094-16100.
[32] Ouellet M, Goyette J, Xiao J. A new approach to optimize the performance of a hydrogen reservoir using activated carbon as the storing material. Int J Hydrogen Energ 2017; 42(38): 24229-24236.
[33] Bai XS, Yang WW, Tang XY, et al. Optimization of tree-shaped fin structures towards enhanced absorption performance of metal hydride hydrogen storage device: a numerical study. Energy 2021; 220: 119738.
[34] Liu L, Wang K, Luo H, et al. Fin structure optimization for improving heat transfer efficiency and hydrogen absorption rate of metal hydride hydrogen storage tank. Int J Hydrogen Energ 2024; 65: 362-374.
[35] Xiao J, Wang J, Cossement D, et al. Finite element model for charge and discharge cycle of activated carbon hydrogen storage. Int J Hydrogen Energ 2012; 37(1): 802-810.
[36] Xiao J, Hu M, Bénard P, et al. Simulation of hydrogen storage tank packed with metal-organic framework. Int J Hydrogen Energ 2013; 38(29): 13000-13010.
[37] Lemmon, E.W., McLinden, M.O., & Friend, D.G. (2013). "Thermophysical Properties of Fluid Systems," in NIST Chemistry WebBook, NIST Standard Reference Database Number 69, Eds. P.J. Linstrom and W.G. Mallard, National Institute of Standards and Technology, Gaithersburg MD, 20899.
[38] Richard MA, Benard P, Chahine R. Gas adsorption process in activated carbon over a wide temperature range above the critical point. Part 1: modified Dubinine-Astakhov model. Adsorption 2009; 15: 43-51.